RSC Advances

ROYAL SOCIETY OF CHEMISTRY

www.rsc.org/advances

Graphic Abstract

A novel tetraethylenepentamine functionalized polymeric adsorbent with polymethacrylate-divinylbenzene as the substrate was facilely prepared for the enhanced removal and selective recovery of Cu(II) and Ni(II) from saline solutions.

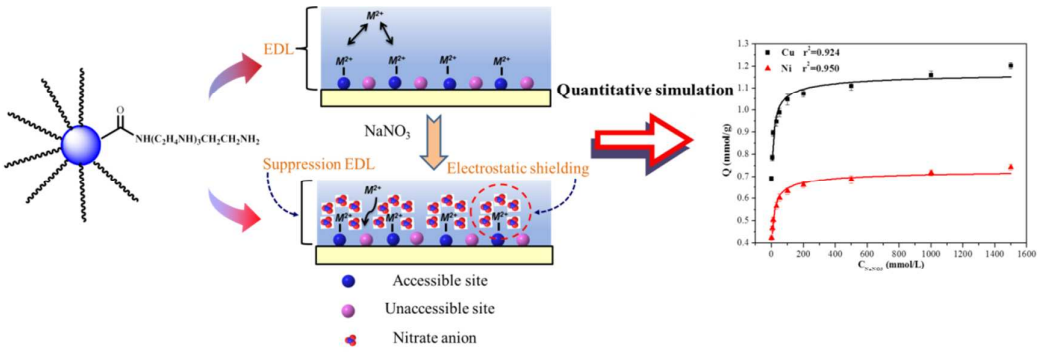

Journal Name

ARTICLE

A novel tetraethylenepentamine functionalized polymeric adsorbent for enhanced removal and selective recovery of heavy metal ions from saline solutions

Received 00th January 20xx,
Accepted 00th January 20xx

DOI: 10.1039/x0xx00000x

www.rsc.org/

Xiao-Peng Zhang,[ab] Fu-Qiang Liu,*[a] Chang-Qing Zhu,[a] Chao Xu,[a] Da Chen,[a] Meng-Meng Wei,[a] Jian Liu,[b] Cheng-Hui Li,[b] Chen Ling,[a] Ai-Min Li[a] and Xiao-Zeng You[b]

A series of multi-amine functionalized polymeric adsorbents with polymethacrylate-divinylbenzene as the substrate were facilely prepared for the enhanced removal and selective recovery of Cu(II) and Ni(II) from saline solutions. The optimal experiment of suspension polymerization between divinylbenzene and methylacrylate was designed by response surface methodology. The multi-amine was successfully grafted on polymethacrylate-divinylbenzene beads as evidenced by N-H deformation vibrations in Fourier-transform infrared spectrometry and characteristic absorption peaks of nitrogen in X-ray photoelectron spectroscopy. Among the newly-synthesized multi-amine adsorbents, the tetraethylenepentamine decorated resin (PAMD) exhibited the highest content of N, reaching as high as 20.38%. The maximum adsorption capacity of PAMD for Cu(II) was up to 1.21 mmol/g, which is obviously superior to such commercial multi-amine resin as Purolite S984. With increasing concentration of $NaNO_3$ in solutions, the uptake of Cu(II) and Ni(II) onto PAMD was significantly enhanced by up to 74.28% and 75.51%, respectively. It is noteworthy that the separation factor towards Cu(II) became infinite with the help of $NaNO_3$ despite the moderate one (1160.19) in Cu(II)/Ni(II) salt-free solution, and such interesting characteristics could be potentially applied to prepare high-purity nickel. The salt-promotion effect of PAMD was expressed by the promotion index (K_P). Furthermore, based on the model of compressed electric double layer, the quantitative simulation of salt-enhanced adsorption was illuminated for the first time. PAMD has also been successfully applied to treat the actual saline effluent, and more volumes of wastewaters can be decontaminated by PAMD (330 BV) compared with S984 (220 BV) under the same condition. These interesting findings suggest that PAMD could be satisfactorily applied in the advanced treatment of actual saline effluents with low-cost, high-efficiency and good-reproducibility.

1. Introduction

During decades, increasing attention has been paid to efficient removal and selective recovery of heavy metals from wastewaters due to both serious environmental issues and potential economic benefits.[1-4] Heavy metals are important strategic resources as well as essential raw materials in the advanced functional material field, such as copper is a key component in electrical and semiconductor device,[5-7] and nickel compounds are used as high-performance catalysts.[8-10] Whereas, heavy metal ions are demonstrated to be highly carcinogenic and toxic to living organism even in trace amounts. For instance, excess copper would cause gastrointestinal distress in short term exposure, and liver or kidney damage in long term exposure.[11] Toxic effluents involving heavy metal ions are always originated from mining, electroplating, chemical, and battery manufacture industries, and frequently a variety of heavy metal ions coexist with high-concentration inorganic salts (alkali or alkaline-earth metal salts).[12-15] Because of interferential effects of substantial inorganic salts, heavy metal ions could not be selectively removed from saline solutions by traditional treatment technologies to meet the strict discharge standard. In that case, residual heavy metal ions may pose great threat to public health and ecosystems. Therefore, it is of great research and practical interest to develop novel technologies as well as advanced materials for removal and recovery of heavy metals from saline effluents.

Adsorption has been proven to be one of the most efficient methods for removal of toxic heavy metal ions from wastewaters because of large capacity, low cost, environmental friendliness and absence of secondary pollution.[16-20] A number of natural and synthetic adsorbents incorporating various functional groups (polyamine, carboxylate, sulphate, iminodiacetate, thiol, aminophosphonate and so on) have been extensively explored.[21-27] In particular, benefiting from exceptional binding abilities of the amine functional group and multiple chelation sites, multi-amine grafted adsorbents present an impressive adsorption capacity and have attracted considerable interest in efficient removal of trace heavy metals from wastewaters.[28-32] Chen et al. reported a novel

[a] State Key Laboratory of Pollution Control and Resource Reuse, School of the Environment, Nanjing University, Nanjing 210046, People's Republic of China, E-mail: jogia@163.com; Fax: +86-25-89680377; Tel: *+86-25-89680377*
[b] State Key laboratory of Coordination Chemistry, School of Chemistry and Chemical Engineering, Collaborative Innovation Center of Advanced Microstructures, Nanjing university, Nanjing 210093, People's Republic of China
† Electronic Supplementary Information (ESI) available. See DOI: 10.1039/x0xx00000x

polyvinyltetrazole-grafted resin with high capacity for adsorption of Pb(II), Cu(II) and Cr(III) ions from aqueous solutions and investigated the effects of pH and salt concentration on the adsorption.[33] Wang et al. synthesized interesting core-shell magnetic Fe_3O_4@poly(*m*-phenylenediamine) particles for chromium reduction and adsorption.[34] Furthermore, according to the theory of hard-soft-acid-base, N atom, a middle partial hard base, favors formation of inner-sphere surface complexes with intermediate partial hard acids, therefore contributing to the unique selectivity of multi-amine functionalized adsorbents. In a saline system, multi-amine adsorbents would bind with heavy metal ions (partial hard acids) preferentially compared to Na(I), K(I), Ca(II) and Mg(II) ions (hard acids).[35-39] As a result, multi-amine adsorbents are capable of efficiently removing and exclusively recovering trace heavy metals from saline wastewaters or other complex wastewaters.

To date, although a great number of multi-amine adsorbents have been reported, their adsorption capacity and selectivity fail to meet increasingly strict discharge standards, and few literatures are devoted to the quantitative examination of salt effects on adsorption performance. Moreover, the treatment of actual saline waste streams has seldom been reported.[40] Therefore, it is of great importance to explore more excellent multi-amine adsorbents and unveil the mechanism of quantitative removal in saline systems for practical treatment of complicated saline wastewaters.

We have previously reported a number of amine-functionalized resins based on styrene-divinylbenzene copolymer and studied their selective adsorption performances in saline solutions.[38,39] In this study, a series of multi-amine functionalized polymeric adsorbents with higher adsorption capacity and selectivity was prepared through amination of polymethacrylate-divinylbenzene micro-beads. Notably, the tetraethylenepentamine decorated resin (PAMD) showed an unprecedented content of N (20.38%) and a large adsorption capacity for heavy metals, e.g. the uptake amount of Cu(II) reached up to 1.21 mmol/g. In addition, the substrate skeleton of PAMD based on methacrylate was demonstrated to be hydrophilic, therefore resulting in a fast adsorption rate, especially in saline solutions. The selective adsorption behaviors for Cu(II) and Ni(II) were examined in salt-free and saline systems. Based on the model of compressed electric double layer (EDL), the salt-enhanced mechanism was quantitatively simulated. This novel multi-amine adsorbent PAMD enjoying exceptional adsorption properties and salt-enhanced effect may be applicable to salt-controlled separation of heavy metals and salt-tuned integrative techniques.

2. Experimental Section

2.1 Materials

All organic reagents including methylacrylate (97%, stabilized with inhibitor), divinylbenzene, benzoyl peroxide, diethylenetriamine (DETA), triethylenetetramine (TETA), tetraethylenepentamine (TEPA), polyethylenepolyamine (PEPA) and cyclohexanol, and all of inorganic reagents were obtained from Nanjing Chemical Reagent Co., Ltd. (Jiangsu Province, PR China). All solutions were prepared using ultrapure water produced by a Millipore-Q system (Millipore Synergy, USA). Commercial resins Purolite S984, D001, Amberlite 747 and Amberlite 748 were obtained from Tianjin Weide International Trade Co., Ltd.

2.2 Preparation of polymethacrylate-divinylbenzene beads (PAM)

A 120 mL amount of 1% (w/v) divinylbenzene cyclohexanol solution was added into the 250 mL three-necked round bottle flask equipped with a mechanical stirrer and a reflux condenser, stirring and heating to 348 K under nitrogen atmosphere. Then, a mixture of 10 mL methylacrylate and 20 mL cyclohexanol (in which 0.2 g benzoyl peroxide was dissolved) was added slowly into the flask, and the suspension polymerization in the flask was allowed to proceed at 348 K for 12 h under nitrogen atmosphere and with stirring at 225 rpm/min. Polymeric beads with sizes in the range of 80-200 μm were formed in the flask and were finally separated via a Buchner funnel. The micro granules were washed with ethanol and ultrapure water, and dried in a vacuum oven at 323 K prior to further use.

2.3 Preparation of multi-amine resins

10 g of polymeric beads (PAM) and 120 mL of corresponding multi-amines (DETA, TETA, TEPA or PEPA) were added into a three-necked round bottle flask, and polymeric beads were swelled for 10 h at the room temperature. Then, the reaction in the 250 mL three-necked round bottle flask was allowed to proceed at 393 K in an oil bath with gentle stirring for 24 h, and the amine functionalized polymeric beads in the bottle were separated by filtration with a Buchner funnel and repeatedly washed with ultrapure water till the pH of the washing water became about the same as the fresh ultrapure water. The multi-amine beads were dried in a vacuum dryer at 313 K to a constant weight and later used as the adsorbent in the adsorption study.

2.4 Characterization of multi-amine resins

Elemental analysis (EA, Vario MICRO Analyzer, Germany) and Fourier transform infrared spectroscopy (FT-IR, NEXUS 870, America) were used to analyze chelating functional groups of the resin. The specific surface area and porous texture of adsorbents was determined by N_2 isotherms data at 77 K using an adsorption analyzer ASAP 2020 (Micromeritics Instrument Co., USA), and calculated with Brunauer-Emmett-Teller (BET) and Dubinin-Radushkevich (DR) methods. Surface chemical states of the resin before and after the interaction with metal ions were further analyzed by X-ray photoelectron spectrometer (XPS) (ESCALAB-2, Great Britain) and the XPSPEAK41 software. Binding energies in the XPS spectra refer to the neutral C1s peak at 284.6 eV to compensate for the surface charging effects and systematic errors.[41] The ζ -potential was measured by a Zeta-Plus4 analyzer (Brookhaven Co., USA). The thermal gravity analysis (TGA) characterization was conducted to investigate the thermal property of PAMD using a thermal analyser (PerKinElmer, USA).

2.5 Adsorption feature of resin

2.5.1 Static adsorption experiments. To evaluate the effect of solution pH on adsorption performance, static experiments were carried out in batch mode and in triplicate by mixing 0.025 g resin with 50 mL of solution containing various defined initial concentrations of Cu(II) and Ni(II) at pH 1, 2, 3, 4 and 5. And adsorption isotherm experiments were conducted at pH 3 with initial concentrations of Cu(II) and Ni(II) being 0.5-5 mmol/L. In salty systems, 0.025 g polyamine resin was added into 50 mL of solutions containing corresponding metal ions in 150 mL conical flasks, and a series of inorganic salts with various concentration ratios were introduced at pH 3. Then the vials were shaken in an incubator shaker at 303 K and 120 rpm for 24 h, and the residual

concentrations of the metal ions were analyzed with a flame atomic absorption spectrophotometer (THERMO, USA).

The quantities of adsorbed metal ions per unit mass of the beads were calculated by eqn (1) and the promotion ratio (P_r) or inhibition ratio (I_r) induced by inorganic salts was determined by eqn (2).

$$Q_e = \frac{(C_0 - C_e) \times V}{W} \quad (1)$$

$$P_r = \frac{Q'_e - Q_e}{Q_e} \times 100\% \text{ Or } I_r = \frac{Q_e - Q'_e}{Q'_e} \times 100\% \quad (2)$$

Where C_0 and C_e (mmol/L) are the initial and equilibrium concentrations of metal ions in the aqueous phase, respectively; V (L) is the volume of aqueous phase; W (g) is the amount of resin and Q_e (mmol/g) is the equilibrium adsorption capacity. Q'_e (mmol/g) is the equilibrium adsorption capacity in saline system. The separation factor α_{Ni}^{Cu} is expressed as eqn (3).

$$\alpha_{Ni}^{Cu} = \frac{Q_{e,Cu}/C_{e,Cu}}{Q_{e,Ni}/C_{e,Ni}} \quad (3)$$

Furthermore, Langmuir and Freundlich models were both applied to describe isotherm data in single systems with the forms of eqn (4) and eqn (5).

$$\frac{C_e}{Q_e} = \frac{C_e}{Q_0} + \frac{1}{Q_0 b} \quad (4)$$

$$Q_e = K_f C_e^{1/n} \quad (5)$$

Where b (L/mmol) is the affinity parameter or Langmuir adsorption constant which reflects the free energy of adsorption; K_f and n are the constant isotherm parameters; and Q_0 (mmol/g) is the capacity parameter.[42]

Binary systems and ternary systems in this section were described by the extended Langmuir model and the modified Langmuir model with the forms of eqn (6) and eqn (7).[43-45] Three-dimensional isotherm images were created by MATLAB with the minimum residual sum of squares (RSS) expressed as eqn (8).

$$Q_{e,i} = \frac{Q_{m,i} K_i (C_{e,i}/\eta_i)}{1 + K_i (C_{e,i}/\eta_i) + K_j (C_{e,j}/\eta_j)} \quad (6)$$

$$Q_{e,i} = \frac{Q_{max} K_{EL,i} C_{e,i}}{1 + K_{EL,i} C_{e,i} + K_{EL,j} C_{e,j}} \quad (7)$$

$$\mathrm{RSS} = \sum_{i=1}^{n} (Q_{ei,fit} - Q_{ei,exp})^2 \quad (8)$$

Where $Q_{m,i}$ and K_i are the maximum capacity and the Langmuir adsorption constant is derived from the corresponding single-component Langmuir isotherm, respectively. Q_{max} and $K_{EL,i}$ are calculated from eqn (7), while η_i and η_j are correction parameters.

2.5.2 Kinetic adsorption experiments. The kinetic adsorption experiments were conducted with $NaNO_3$ as the background electrolyte at solution pH 3 in Cu(II) single system, Cu(II)/Ni(II) binary system and Cu(II)/Ni(II)/$NaNO_3$ ternary system. The concentration of each heavy metal was 1 mmol/L in all systems. Briefly, 1000 mL of solution with 0.125 g PAMD was agitated at 120 rpm and 303 K in an incubator shaker, during which they were sampled at pre-defined time intervals. The pseudo-first-order rate equation (eqn (9)) and pseudo-second-order rate equation (eqn (10)) given as the following non-linear forms were both used to describe the kinetic adsorption process.

$$\log(Q_e - Q_t) = \log Q_e - \frac{k_1 t}{2.303} \quad (9)$$

$$Q_t = \frac{k_2 Q_e^2 t}{1 + k_2 Q_e t} \quad (10)$$

Where Q_t is the adsorption capacity at time t (mmol/g); k_1 and k_2 are the rate constants of pseudo-first-order (min^{-1}) and pseudo-second-order (g $mmol^{-1}$ min^{-1}), respectively. And $h = k_2 Q_e^2$ is defined as the initial adsorption rate constant.[46]

2.5.3 Dynamic adsorption. About 0.5 g (2.4 mL) of PAMD was placed in a glass column (Φ 10×240 mm). Solution of metal ions at initial concentration of 1.0 mmol/L was controlled to flow gradually through the glass column at a rate of 10 BV/h (bed volume per hour) and 303 K, and the concentrations of background electrolyte ranged from 0 to 1500 mmol/L. The resin bed was regenerated with 15% HCl solution in 2 BV/h downward flow at room temperature until Cu(II) or Ni(II) was not detected in the effluent. Aliquots of the effluent (C_e) were taken at regular time intervals to determine the concentration of Cu(II) or Ni(II) in the effluent. The breakthrough point and saturation point of the column were defined at $c_e/c_0 = 0.05$ and $c_e/c_0 = 0.9$, respectively.

3. Results and discussion

3.1 Preparation of multi-amine resins

Multi-amine resins were prepared via the amination of polymethacrylate-divinylbenzene (PAM) beads with corresponding multi-amines, and all the raw materials were low-cost and facile. Various multi-amines with different chain lengths were selected to modify the PAM beads. The resin PAMB was obtained with DETA as the reagent, and PAMC, PAMD, PAMN corresponded to TETA, TEPA, PEPA, respectively. The synthetic route is shown in Scheme 1.

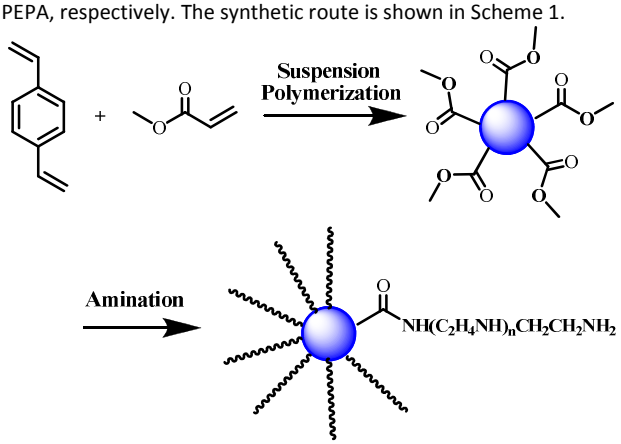

Scheme 1 Synthetic route for the preparation of multi-amine resins.

Compared to the preparation of chloromethylated styrene-divinylbenzene copolymer beads, the synthesis of PAM substrate is more facile and green, and the poisonous reagent chloromethyl methyl ether can be avoided.[47] In the synthesis process of PAM, polymerization temperature, reacting time and stirring speed have a significant impact on the size of beads, the amount of modified functional group and adsorption behaviors of obtained multi-amine resins. Accordingly, we have utilized response surface methodology (RSM) to optimize the reaction conditions of polymerization.[48] Different temperatures, reacting times and stirring speeds were attempted to prepare the PAM, and the relationship between reaction conditions and adsorption behaviors of a series of PAMD resins synthesized from different PAM beads was examined. As shown in Fig. 1, according to the three-dimensional response surface plots, the optimal reaction temperature, time and speed were selected at 348 K, 12 h and 225 rpm/min, respectively. Under this condition, 80-200 μm multi-amine microspheres can be succefully seperated and a large adsorption capacity of Cu(II) can be obtianed.

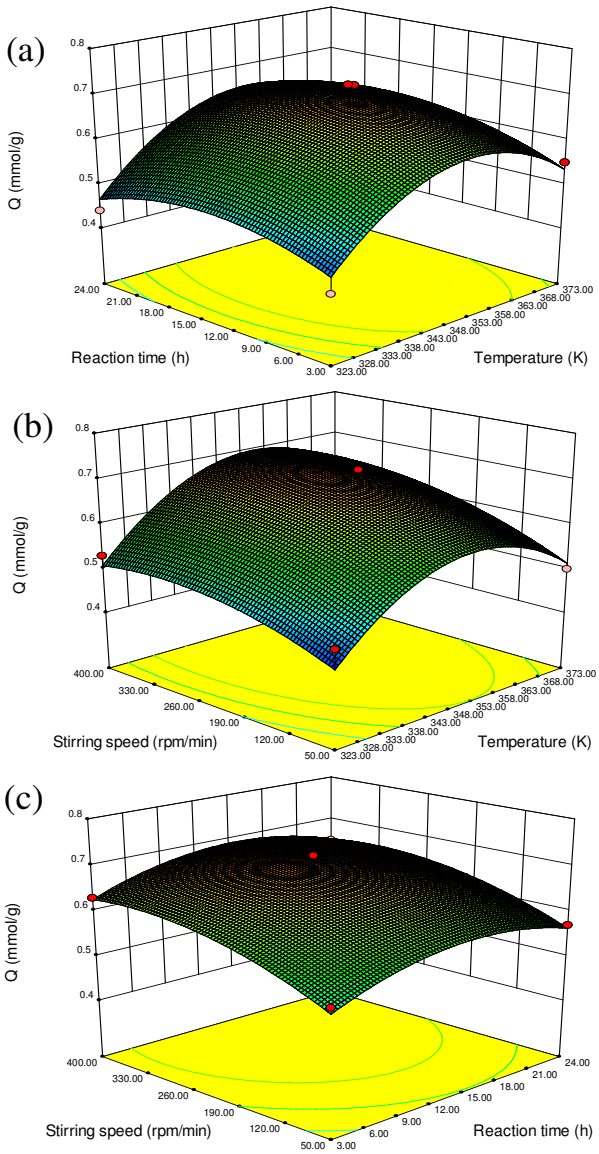

Fig. 1 Response surfaces for Cu(II) removal: (a) reaction time –temperature; (b) stirring speed – temperature; (c) stirring speed – reaction time.

In the following reaction of decorating multi-amine, to ensure that almost all the available ester groups have been aminated, different temperatures and times were regulated. It was found that reacting at 393 K for 24 h was perferable, and elevating temperature and prolonging reaction time can not increase the adsorption performance of multi-amine resins.

3.2 Characterization of multi-amine resins

The obtained polymethacrylate-divinylbenzene beads and a series of multi-amine resins was characterized by elemental analysis and Fourier transform infrared spectroscopy (FT-IR). The elemental analysis results of prepared resins were tabulated in Table 1. The tetraethylenepentamine functionalized resin (PAMD) presented the highest content of modified amine (N content: 20.38%), providing an essential prerequisite for attaining a great adsorption performance. In addition, the N content of all self-synthesized multi-amine resins was higher than that of commercial resin S984.

Table 1 EA results of PAM beads and mutli-amine resins

resin	C (%)	H(%)	N (%)
PAM	57.79	7.55	0.34
PAMB	49.15	8.79	18.97
PAMC	53.94	9.19	19.38
PAMD	50.36	9.71	20.38
PAMN	48.77	9.25	17.42
S984	50.22	8.66	17.32

As shown in Fig. 2, the strong FT-IR absorption of all compounds at 1750~1610 cm^{-1} can be assigned to C=O stretching vibration.[49] For PAM, the vibration band of C=O resided at 1737 cm^{-1}. However, after grafting multi-amine, the stretching vibration of N-C=O was red-shifted to 1657 cm^{-1}.[50] In addition, a new absorption band near 1553 cm^{-1} emerged in multi-amine resins, originating from N–H deformation vibration.[38] The specific surface area and porous texture of adsorbents were also examined (Table 2). After amination, the specific surface area, mean pore size and pore volume all increased. For PAMD, the mean pore size was 5.8866 nm and much larger than the hydrated metal ion radius, allowing efficient diffusion of hydrated metal ion into the resin. Furthermore, the TGA measurement of PAMD has been performed (Fig. S1), and no distinct decompositon occured until 190 ˚C, suggesting a good thermal stability.

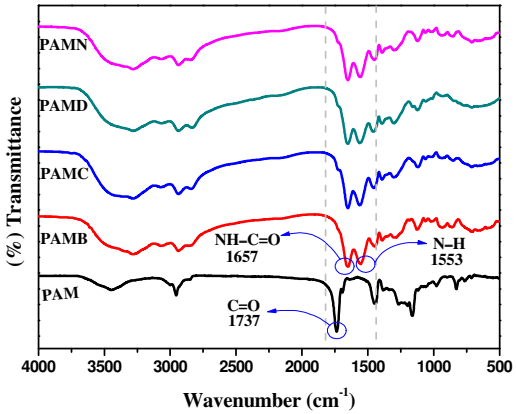

Fig. 2 FT-IR spectra of PAM beads and mutli-amine resins.

Table 2 Specific surface area and porous texture information of PAM beads and mutli-amine resins

resin	S_{BET}(m^2/g)	V_t(cm^3/g)	Pore Size (nm)
PAM	0.7875	0.000226	1.1480
PAMB	0.8263	0.000577	2.8012
PAMC	0.7885	0.000965	4.8963
PAMD	4.7888	0.007047	5.8866
PAMN	0.7024	0.000545	1.9168

3.3 Adsorption of Cu(II) in single systems

To screen the preferred self-synthesized multi-amine resin, the adsorption of Cu(II) in single systems has been carried out (Fig. 3). It can be found that self-synthesized multi-amine chelating resins presented better adsorption behaviors than S984 towards Cu(II) in a proper order: PAMD>PAMC>PAMB>PAMN>S984, which was consistent with the content of amine functional group as revealed from EA results. Compared to PAMB and PAMC, PAMD exhibited a larger adsorption capacity, which was attributed to more chelation sites on tetraethylenepentamine. For PAMN, due to substantial amine groups on polyethylenepolyamine, cross-linking was easy to

be actualized between polyethylenepolyamine and methacrylate. In addition, under serious cross-linking, some ester groups would be enwrapped and could not be aminated availably, leading to a smaller pore size, a lower content of N and corresponding an inferior adsorption performance. Therefore, in the following investigation, we will focus on the adsorption properties of PAMD.

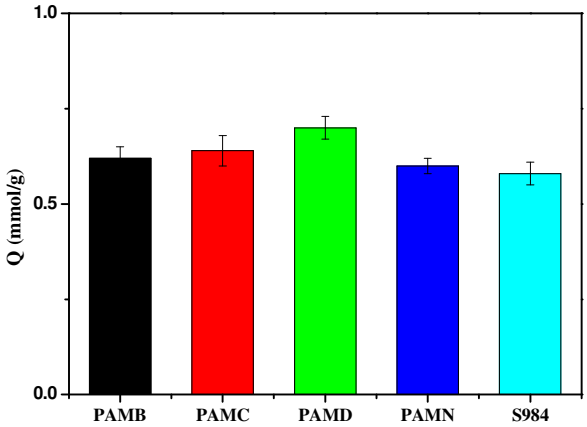

Fig. 3 Adsorption amounts of Cu(II) in single systems.

3.4 Enhanced adsorption in Cu(II)/salt or Ni(II)/salt binary systems

We compared the salt tolerance of PAMD with several commercial ion exchange resins such as D001, Amberlite 747 and Amberlite 748. As shown in Fig. 4, in Cu(II)/salt system, with increasing concentration of inorganic salt, the adsorption capacities of commercial ion exchange resins such as D001, Amberlite 747 and Amberlite 748 decreased dramatically. D001 resin was even deprived of the adsorption ability (I_r = 99.84%) at high concentrations of inorganic salts. Because ion exchange adsorbents benefited formation of outer-sphere surface complexes with heavy metals through electrostatic attraction, the adsorption performances of which were susceptible to site competition of alkali or alkaline-earth metal ions in the background electrolyte.[14,51] In contrast, the amine-functionalized resins utilizing a complexiметric mode bound heavy metals preferentially over alkali/alkaline earth metal ions, so the site competition could be neglected.[38,39] Compared to the commercial polyamine resin S984, PAMD presented higher adsorption capacity and stronger salt-promotion effect due to super-high content of modified amine groups. Dependence of the adsorption performance of PAMD on salt species was further investigated (Fig. S2-S5). Among all the selected inorganic salts, Cl^- and SO_4^{2-} exerted less evident promotion effects than NO_3^- did, which can be rationalized by the complexation effect of Cl^- and the large steric hindrance of SO_4^{2-}.[40,52] For various alkali or earth alkali cations, sodium salt presented the best effect of salt-promotion, so $NaNO_3$ served as the background electrolyte in the following experiments. Furthermore, the influence of Cr(VI) anions on the adsorption performance of Cu(II) has been explored, and a positive salt-enhanced effect was presented. In the presence of 5 mmol/L Cr(VI) anions, the adsorption capacity of Cu(II) was promoted by 12.45%. Due to the strong oxidizing property of Cr(VI), redox reactions may happen at the interface of adsorbent, and Cr(VI) would be transformed into Cr(III). The in-depth investigation involving the synergistic removal of toxic heavy metal ions Cr(VI) and Cu(II) will be reported before long.

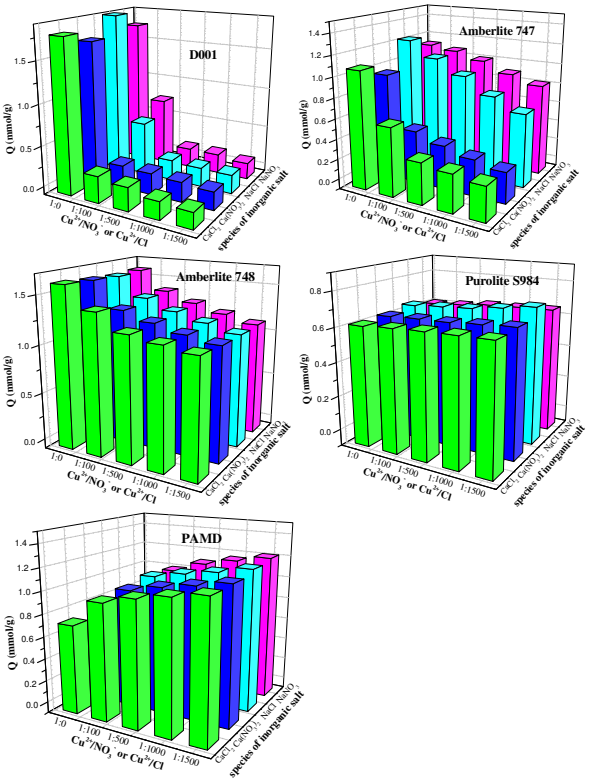

Fig. 4 Adsorption amounts of Cu(II) in saline systems with different concentrations of inorganic salts.

The pH-dependent adsorption behaviors of PAMD were also explored in single system, as well as Cu(II)/$NaNO_3$ and Ni(II)/$NaNO_3$ systems (Fig. S6-S7). Due to weak basicity of amine groups, nitrogen sites were easily protonated through adsorbing hydrogen ions in the acidic solution, so there would be a site competition between H^+ and Cu(II). When pH was higher than 2.5, the uptake amount of Cu(II) increased with rising concentration of $NaNO_3$, showing a prominent salt-enhanced effect (Fig. S7). However, the adsorption of Cu(II) was suppressed by salts under pH 2.5. At a lower H^+ concentration, the adsorption of Cu(II), as an advantageous component binding with nitrogen sites, was promoted with $NaNO_3$. Whereas, as the concentration of H^+ increased, the active sites of PAMD bound hydrogen ions preferentially, which was enhanced by introducing $NaNO_3$ because of compressed EDL effect and electrostatic shielding effect exerted by anions. The adsorption performance of Ni(II) as a function of aqueous pH changed similarly to that of Cu(II), while the pH threshold between salt-enhanced and salt-suppressed effects was 2.6 due to the weaker binding affinity between amine groups and Ni(II) ions (Fig. S7).[35,53]

3.5 Adsorption and separation in Cu(II)/Ni(II)/$NaNO_3$ ternary systems

In Cu(II)/Ni(II)/$NaNO_3$ ternary system, the isotherm of Ni(II) was curved concavely downward with elevating concentration of Cu(II), whereas the adsorption surface of Cu(II) was insensitive to the concentration of Ni(II) (Fig. 5). With increasing concentration of $NaNO_3$, more Cu(II) ions were sequestrated onto PAMD, while the uptake amount of Ni(II) decreased, revealing that coexisting inorganic salts boosted the adsorption capacity of favorable component and correspondingly improved the selective separation

performance. When the initial concentrations of Cu(II) and Ni(II) were both fixed at 1 mmol/L, the adsorption capacity of Cu(II) was promoted by 27.81%, 50.79% and 73.65% with 10, 100 and 1500 mmol/L $NaNO_3$, respectively. However, the adsorption of Ni(II) was suppressed significantly, and the uptake amount was less than 0.1 mmol/g, with the inhibitory effect intensified at higher $NaNO_3$ concentration.

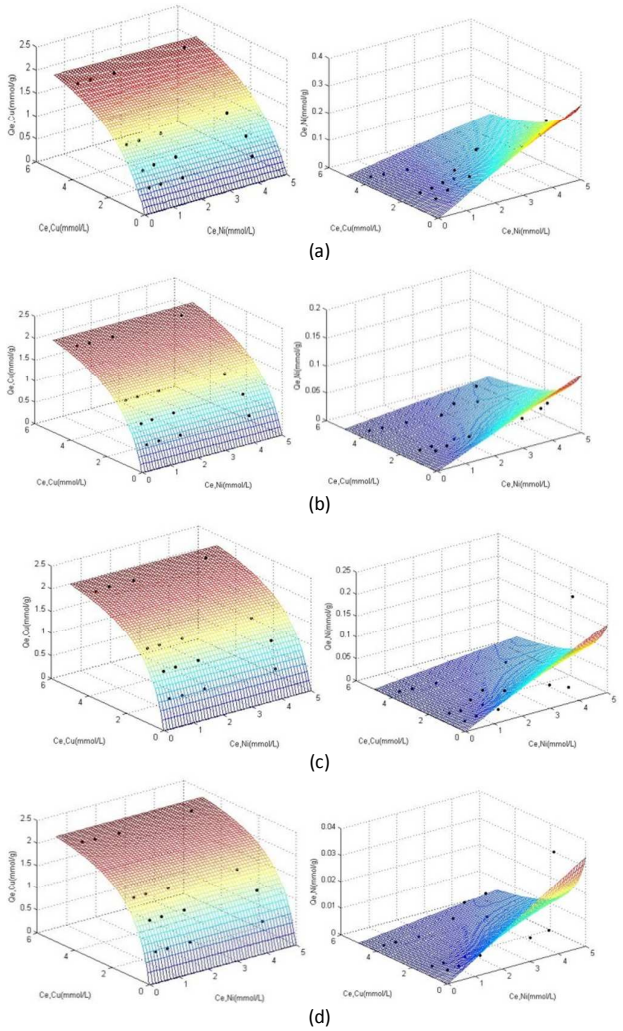

Fig. 5 Three-dimensional isotherm surfaces of PAMD simulated with the extended Langmuir model from: (a) Cu(II)/Ni(II) binary systems, (b) Cu(II)/Ni(II)/$NaNO_3$ (10 mmol/L) ternary systems, (c) Cu(II)/Ni(II)/$NaNO_3$ (100 mmol/L) ternary systems, (d) Cu(II)/Ni(II)/$NaNO_3$ (1500 mmol/L) ternary systems.

For uptake of each species in Cu(II)/Ni(II) binary and Cu(II)/Ni(II)/$NaNO_3$ ternary systems, the extended Langmuir model describes the experimental data better than the modified Langmuir model does, with lower residual sum of squares (RSS) values (Fig. 5, Fig. S8 and Table S1). Compared to Ni(II), the simulated η (inhibitory effect of metal ion on the adsorption of other species) and $K_{EL,i}$ (affinity of polyamine resins toward the adsorbates) values of Cu(II) were lower and higher respectively.[54] As a result, Cu(II), as the dominant, favorable adsorptive component, suppressed Ni(II) sequestration more markedly. The maximum adsorption capacity $Q_{\max}$ and the affinity coefficient K_{Cu} increased with elevating concentration of $NaNO_3$, whereas K_{Ni} was depressed distinctly, rendering K_{Cu}/K_{Ni} ratio to increase significantly up to 406.17 in 1500 mmol/L $NaNO_3$ solution. As shown in Table S1, the calculated maximum adsorption capacity for Cu(II) in highly saline systems (1500 mmol/L $NaNO_3$) is 2.90 mmol/g, which is comparative to our previous work (1.35 mmol/g, aminothiazole-functionalized chelating resin;[38] 1.738 mmol/g, dual-primary-amine chelating resin[39]) and those reported amine-grafted adsorbents (0.52 mmol/g, amino-functionalized modified metal ion imprinting adsorbent;[30] 0.81 mmol/g, silica-aminomethyl pyridine adsorbent;[53] 1.32 mmol/g, diethylenetriamine-functionalized adsorbent;[55] 1.76 mmol/g, chitosan adsorbent;[36] 2.98 mmol/g, polyvinyltetrazole-grafted resin[33]).

The separation factors α_{Ni}^{Cu} in Cu(II)/Ni(II) binary and Cu(II)/Ni(II)/$NaNO_3$ ternary systems were investigated (Table S2). Regardless of $NaNO_3$ concentration, the values of α_{Ni}^{Cu} all exceeded 1, suggesting that Cu(II) was the preferable component and adsorbed preferentially relative to Ni(II). With Cu(II) and Ni(II) being at the same initial concentrations, α_{Ni}^{Cu} increased with rising concentration of $NaNO_3$. After $NaNO_3$ was introduced, EDL became thinner and more active complexation sites were available on the resin.[52] As revealed by the values of η_{Cu} and η_{Ni}, Cu(II) had a strong antagonistic effect on the adsorption of Ni(II), while the suppressive influence of Ni(II) on Cu(II) was negligible. Thus, α_{Ni}^{Cu} increased notably and became infinite in 1500 mmol/L $NaNO_3$ solution.

3.6 Accelerated kinetics in saline solutions

The kinetic adsorption performances of Cu(II) and Ni(II) in various static systems with or without $NaNO_3$ were examined (Fig. S9). The equilibrium time was 1440 minutes and the kinetic adsorption behaviors were well simulated (Table S3). The initial adsorption rate and adsorption capacity of Cu(II) were elevated distinctly with increasing concentration of $NaNO_3$, resulting in remarkable exclusive removal and selective sequestration of Cu(II) in the saline system. Nevertheless, Ni(II), as the disadvantageous component, was inhibited more significantly in a more salty solution.

The kinetics of H^+ uptake and time course of pH were investigated as well (Fig. S10-S11). For both non-salt and saline systems, the uptake of hydrogen ion was far faster than that of copper ion initially (Fig. S10). During adsorption, the mole ratio of adsorbed H^+ to Cu(II) decreased from 411.32 to 6.11 in the salt-free solution, and from 24.63 to 4.16 in the saline system. At equilibrium, pH of the saline system was slightly higher than that of the salt-free solution (Fig. S11), suggesting more hydrogen ions were adsorbed in the presence of inorganic salts. Similarly, Navarro et al. reported that metal sequestration and protonation were both enhanced in saline system due to significant stimulation effect of abundant anions, and that there were sufficient available sites, allowing sequestration of H^+ and Cu(II) simultaneously.[40]

3.7 Dynamic separation and regeneration

The dynamic adsorption behaviors of Cu(II)/Ni(II) with or without $NaNO_3$ were explored (Fig. S12 and Table S4). In the single system, the breakthrough point ($c_e/c_0 = 0.05$) and saturation point ($c_e/c_0 = 0.9$) for Cu(II) were 92 BV and 332 BV, respectively, while the values were 4 BV and 244 BV for Ni(II). In the Cu(II)/Ni(II) binary system, the breakthrough point increased to 120 BV for Cu(II) while decreased to 1 BV for Ni(II). In the Cu(II)/Ni(II)/$NaNO_3$ ternary system, with increasing concentration of $NaNO_3$, the breakthrough point increased for Cu(II) while decreased more significantly for

Ni(II). In 100 mmol/L $NaNO_3$ solution, the breakthrough point and saturation point of Ni(II) plummeted to 0.5 BV and 64 BV, respectively, but the breakthrough point of Cu(II) increased to 152 BV. Thus, Cu(II) and Ni(II) could be efficiently separated in 64–152 BV. In the ternary solution containing 1500 mmol/L $NaNO_3$, the separation efficiency was further augmented and the effluent of highly pure Ni(II) was obtained from 56 to 172 BV.

The desorption performance of adsorbent is also important in practical applications. The experiments for desorption efficiency were carried out with 15% HCl at the rate of 2 BV/h and 303 K in Cu(II)/Ni(II) sole system. The results of elution experiments for Cu(II) and Ni(II) were shown in Fig. S13. The concentrations of both Cu(II) and Ni(II) eluents were peaked at 5 BV. For Cu(II) and Ni(II), the desorption process was basically done at 20 BV.

In order to investigate the stability and regeneration ability of PAMD, Cu(II) solution at initial concentration of 1.0 mmol/L was controlled to flow gradually through the glass column at the rate of 5 BV/h and 303 K. The experiments for desorption efficiency were carried out with 15% HCl at the rate of 2 BV/h and 303 K. Then the glass column was rinsed thoroughly with distilled water until the effluent was neutral. The procedures described above were repeated 3 times (Fig. S14). The saturation points for Cu(II) were 324 BV, 332 BV and 328 BV, indicating that PAMD could remain chemically stable after being regenerated and reused for many times. The exceptional selectivity and chemical stability suggest that PAMD could be potentially applied in the preparation of high-purity nickel.

3.8 Adsorption mechanisms and simulation

3.8.1 Qualitative elucidation. In order to unveil the adsorption mechanisms, the surface interactions involved in adsorption were examined by Fourier transform infrared spectroscopy (FT-IR), X-ray photoelectron spectrometer (XPS) and density functional theory (DFT) calculation. As displayed in Fig. S15, the band at 1553 cm^{-1} in FT-IR spectra shows an attenuation in intensity for PAMD-Cu(II) and PAMD-Ni(II) compared to PAMD, which is assigned to the deformation vibrations of N-H bond in secondary amine.[38] It can be speculated that nitrogen atoms formed a coordination bond with Cu(II)/Ni(II). Moreover, nitrate anions were simultaneously adsorbed for charge balance in PAMD-Cu(II) and PAMD-Ni(II), revealing a strong stretching vibration at 1384 cm^{-1}.[56]

To further confirm the coordinating interaction between nitrogen atoms and heavy metal ions, XPS characterizations of PAMD and PAMD-Cu(II) were carried out (Fig. S16). From the pictures of wide scans, three peaks, denoting C 1s (284.6 eV), N 1s (399 eV) and O 1s (531 eV), were observed for both PAMD and PAMD-Cu(II). In addition, a distinguishable peak at 933 eV corresponding to Cu 2p was showed in PAMD-Cu(II). The N 1s core-level XPS spectrum were deconvoluted into two peaks at binding energies of 399.01 and 400.91 eV for PAMD, which were ascribed to the nitrogen in the neutral amine (–NH_2 or –NH–) and protonated amine (–NH_3^+ or –NH_2^+–), respectively.[55] As expected, the two peaks shifted to higher binding energies at 399.4 eV and 401.1 eV in PAMD-Cu(II), verifying the formation of nitrogen-metal complexes. Furthermore, a new peak emerged at 406.5 eV, which was attributed to nitrogen atoms in NO_3^-.[21] Simultaneously, the binding energy of O 1s almost remained unchanged before and after adsorbing Cu(II) ions, indicating that they did not participated in the formation of coordination bond. The XPS of PAMD-Ni(II) was also explored, and Ni(II) bound with PAMD through coordination interactions between nickel ions and nitrogen atoms (Fig. S16). The XPS results were in line with the analysis of FT-IR, and Cu(II)/Ni(II) were captured by PAMD through forming metal-nitrogen complexes.

The coordination interaction of PAMD with Cu(II) has been investigated by density functional theory (DFT) as well. The Mulliken atomic charge distribution of the long-chain alkylamine ligand resided in the range of -0.860 ~ +0.350 (Fig. S17). The nitrogen atom with more negative charges is able to capture metal ions more effectively due to stronger mutual electro-static attraction and higher coordination affinity. The charges of secondary amine were -0.255, -0.210, -0.256 and -0.280, while a higher negative charge (-0.572) was exhibited for the primary amine, which is more conducive to form a more stable chelating complex. Two probable configurations (Complex-I and Complex-II) were examined (Fig. S18 and Table S5). In consideration of polydentate chelating interaction and macrocyclic effect, the type II was the preferred combination mode.[55,56]

The ζ-potential of PAMD was measured to evaluate the surface electrostatic interactions (Fig. S19). The ζ-potential of PAMD was largely positive at pH-value between 2.0 to 10.0, indicating that a part of neutral amines (–NH_2, –NH–, etc.) in PAMD were present in protonated forms (–NH_3^+, –NH_2^+–, etc.). PAMD had a zero point of ζ-potential at pH 11.6 in salt-free solution, and with increasing the concentration of $NaNO_3$, the ζ-potential reduced. Then the free metal ions in bulk solution could arrive at surface of resin faster in salty system, furthermore, the positive charges of pronated amino groups can be neutralized faster with increasing the concentration of anions, as a consequence the metal sorption rate was accelerated, and the equilibrium came early in the saline solution compared to salt-free system.[40]

During the adsorption of heavy metals, a part of active sites on PAMD were occupied by metal cations and the rest were protonated. Accordingly, electrostatic repulsions were intensified, and free metal cations in solution were prevented from approaching the remaining active sites (Fig. 6).[57] In the saline system, a substantial number of anions exerted a significantly positive effect on the uptake of heavy metals onto PAMD by compressing EDL, shielding the positive charges, weakening the repulsions, releasing more active sites, and dramatically enhancing the adsorption capacity (Fig. 6).[38-40] Moreover, the repulsive interaction was decreased, as evidenced by the gradually reduced ζ-potential with increasing salt concentration.[58]

Journal Name

ARTICLE

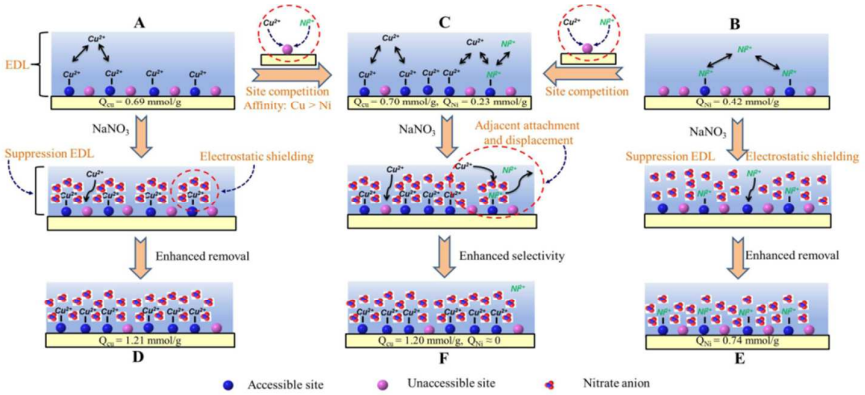

Fig. 6 Qualitative mechanisms behind the salt-enhanced removal and salt-tuned selectivity of Cu(II) (A: Cu(II) single system; B: Ni(II) single system; C: Cu(II)/Ni(II) binary system; D: Cu(II) + 1500 mmol/L $NaNO_3$; E: Ni(II) + 1500 mmol/L $NaNO_3$; F: Cu(II) + Ni(II) + 1500 mmol/L $NaNO_3$).

Adsorption affinity depends on the characteristics of metal ion. Nitrogen atoms, middle partial hard bases, are prone to coordinating with intermediate partial hard acids.[35,55] In comparison with Ni(II), Cu(II) possessed higher absolute electronegativity, log value of first hydrolysis constant and polarization force (Table S6), consequently forming a more stable complex with nitrogen atoms.[38] Therefore, in the binary and ternary systems, Cu(II), as the favorable species, was preferentially scavenged by polyamine resins.

Liu et al. found in competitive adsorption process that displacement interactions were accomplished through an adjacent attachment and repulsion mechanism.[55] With $NaNO_3$, the electrostatic repulsion from adsorbed Ni(II) was attenuated by shielding effects of anions, and then free copper ions in bulk solution approached the adsorbed Ni(II) through an adjacent attachment, where they induced an intense repulsion. Given the weaker binding ability with amine groups, the adsorbed Ni(II) was displaced by Cu(II) and dislodged into bulk solution (Fig. 6), which was more obvious in a more salty solution. Therefore, PAMD was capable of exclusively sequestering Cu(II) in the presence of high-concentration inorganic salts or efficiently removing both Cu(II) and Ni(II) from effluents by lowering inorganic salt concentration. In other words, either selective recovery or synchronous removal was allowed by changing the concentration of inorganic salt, which was verified by the adsorption performances in Cu(II)/Ni(II)/$NaNO_3$ ternary system (Fig. 7). The uptake amount of Cu(II) increased while that of Ni(II) decreased with increasing concentration of $NaNO_3$. Furthermore, total adsorption (sum of uptake of Cu(II) and Ni(II)) was promoted with coexisting $NaNO_3$.

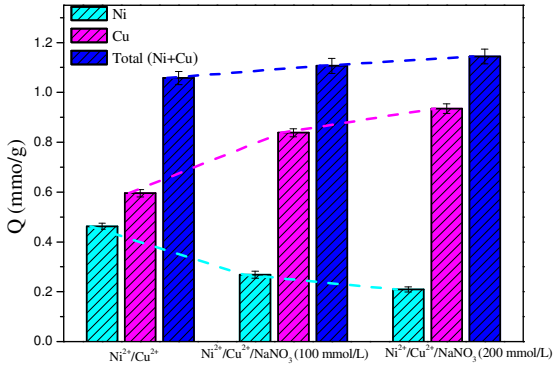

Fig. 7 Adsorption of Cu(II) and Ni(II) in Cu(II)/Ni(II)/$NaNO_3$ ternary system with different concentrations of $NaNO_3$.

In addition, preloading experiments were performed (Fig. S20) by firstly feeding PAMD beads in $Ni(NO_3)_2$ solution (referred to as $PAMD_{Ni}$) to confirm site competition effects. When these Ni(II)-loaded samples were placed in $Ni(NO_3)_2$/$NaNO_3$ (containing 1, 100 and 200 mmol/L $NaNO_3$, respectively) solutions, the adsorption capacity of Ni(II) was enhanced by 8.30%, 23.68%, 30.43% respectively. Nonetheless, as the beads were immersed in sole Cu(II) and Cu(II)/$NaNO_3$ (containing 100 and 200 mmol/L $NaNO_3$, respectively) solutions, 17.66%, 52.12% and 62.92% of the pre-adsorbed Ni(II) ions were displaced by Cu(II) and released into bulk solution. Therefore Cu(II) would suppress the adsorption of Ni(II) more intensely at the higher salt concentration.

3.8.2 Quantitative simulation. The enhancement coefficient is dependent on the concentration of $NaNO_3$ (Fig. S21). At a low concentration, the promotion ratio increased sharply, which, however, became sluggish as the concentration rose. The salt-promoted adsorption process can be divided into two parts. $NaNO_3$ concentration at the inflection point was 100 mmol/L at which P_r was 51.73% for Cu(II). As the concentration of $NaNO_3$ reached 1500

mmol/L, P_r was 74.28%. The enhancement ability of $NaNO_3$ can be described by the promotion index K_P (L/g) (eqn (11)).

$$K_P = \frac{\Delta Q_e}{\Delta C_{NaNO_3}} \quad (11)$$

Where, ΔQ_e (mmol/g) is the increment of metal uptake amount with increasing initial concentration ΔC_{NaNO_3} (mmol/L) of $NaNO_3$. In the low-salt zone (0-10 mmol/L), K_P was 2.05×10^{-2} L/g, implying a strong salt-promotion effect. However, the enhancement effect was weakened in the high-salt zone (100-1500 mmol/L), as evidenced by $K_P$of 1.11×10^{-4} L/g, and salt-promotion exhibited a marginal effect (Fig. 8). For uptake of Ni(II), the salt-enhanced effect was in line with that of Cu(II), and P_r values were 49.35% and 75.51% in solutions containing 100 mmol/L and 1500 mmol/L $NaNO_3$, respectively. K_P of Ni(II) decreased from 8.01×10^{-3} L/g to 7.91×10^{-5} L/g, corresponding to salt concentration zones of 0-10 mmol/L and 100-1500 mmol/L (Fig. 8).

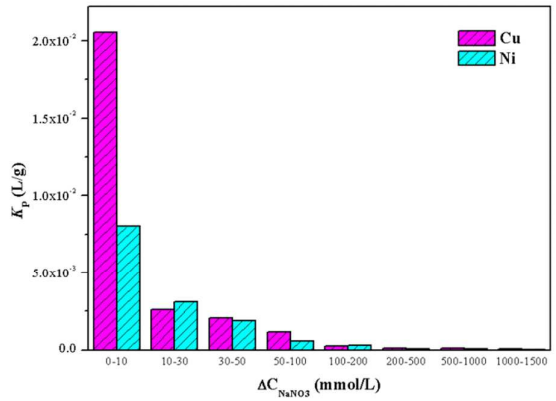

Fig. 8 Promotion indexes (K_P) of Cu(II) and Ni(II) in Cu(II)/Na(I) and Ni(II)/Na(I) binary systems with different concentrations of $NaNO_3$.

According to the Stern EDL model and the triple layer model, the surface of adsorbents is always negatively or positively charged, to which hydrated counterions are electrostatically attracted, forming interfaces known as "inner Helmholtz plane (IHP)" and "outer Helmholtz plane (OHP)" that differ in the orientation of hydrated counterions (Fig. S22).[59] Inside IHP, counteranions are specifically adsorbed to interact closely with the surface charges, while those in between IHP and OHP are nonspecifically adsorbed. In addition, the zone from the surface of adsorbents up to OHP is known as the Stern layer. The region outside OHP is called "diffuse layer" in which counterions tend to diffuse away from the surface to the bulk solution. Therefore, OHP is specified as the boundary to distinguish the fixed and mobile parts of the diffuse double layer.

In saline systems, EDL is compressed more markedly with increasing concentration and valence of ions of opposite sign to that of the surface charge.[60] Furthermore, the potential (ψ) decreases linearly in the Stern layer from its surface potential (ψ_0) to the Stern potential (ψ_d),[61] after which it falls exponentially. Thereby, ψ in the stern layer can be calculated as eqn (12).

$$\psi = \psi_0 - h\kappa^{-1} \quad (12)$$

Where h is a fixed value, and κ^{-1} is the thickness of EDL calculated as eqn (13).[60]

$$\kappa^{-1} = \sqrt{\frac{\varepsilon_0 RT}{F^2 \sum_{i=n} c_i z_i^2}} \quad (13)$$

Where: F is the Faraday constant; c_i the electrolyte concentration; z_i is the valence of ion i; ε_0 is the dielectric constant of the medium; R is the gas constant and T is the absolute temperature (K).

Tang et al.[62] and Xiao et al.[63] have quantitatively modeled the adsorption of perfluoroalkyl acids and explored the variations of adsorption free energy in different concentrations of inorganic salts. They found that hydrophobic and electrostatic effects contributed to the total free energy of adsorption ($\Delta G_{adsorption}$), as shown in eqn (14).

$$\Delta G_{adsorption} = \Delta G_{hydrophobic} + \Delta G_{electrostatic;\,adsorbate-adsorbent} + \Delta G_{electrostatic;\,adsorbate-adsorbate} \quad (14)$$

In our system, nitrogen atoms of PAMD bound heavy metals through coordination rather than electrostatic attractions, therefore forming inner-sphere surface complexes. In this case, the active sites of PAMD adsorbing metal cations or hydrogen ions can be treated as an indivisible whole due to chemical bonding (Fig. S22). Moreover, there was no hydrophobic contribution. Thus, coordination and electrostatic interactions synergistically controlled the adsorption process of PAMD. Accordingly, eqn (14) can be derived into:

$$\Delta G_{adsorption} = \Delta G_{complexation} + \Delta G_{electrostatic;adsorbate-adsorbent} \quad (15)$$

Where $\Delta G_{complexation}$ depends on the property and concentration of heavy metals as well as the characteristic of functional groups immobilized on the resin, so it can be considered as a constant in a certain system. Furthermore, $\Delta G_{electrostatic;adsorbate-adsorbent}$ can be calculated as eqn (16)[63]:

$$\Delta G_{electrostatic;adsorbate-adsorbent} = zF\psi \quad (16)$$

When the adsorption reaches equilibrium, $\Delta G_{adsorption}$ can be obtained from the equilibrium constant K_d:

$$\Delta G_{adsorption} = -RT \ln K_d \quad (17)$$

K_d can be calculated by:

$$K_d = \frac{Q_e}{C_e} \quad (18)$$

Where, Q_e (mmol/g) and C_e (mmol/L) are the solid and liquid phase concentrations at equilibrium, respectively. Furthermore, the relationship between Q_e and C_e can be expressed as:

$$C_0 V = Q_e m + C_e V \quad (19)$$

Where, C_0 is the initial concentration of heavy metal ions in solution; m is the mass of resin used in the adsorption experiment and V is the volume of solution.

Hence, on the basis of eqn (12)-(19), the correlation between Q_e and c_i can be approximated as:

$$Q_e = \frac{Q_0}{m + Ve^{\frac{\Delta G_{complexation} + zF(\varphi_0 - h\sqrt{\frac{\varepsilon_0 RT}{F^2 \sum_{i=n} c_i z_i^2}})}{RT}}} \quad (20)$$

Where, for a certain adsorption system, the values of Q_0, m, V, $\Delta G_{complexation}$, z, F, φ_0, h, ε_0, R, T and z_i are all fixed. It is noteworthy that adsorption behaviors of Cu(II) and Ni(II) in saline systems can be described well by eqn (20), with r^2 being 0.924 and 0.950, respectively (Fig. 9). Therefore, the salt-enhanced adsorption of heavy metals by PAMD can be quantitatively modeled by eqn (20) based on the compression effect of EDL, which may provide valuable reference for clarifying the salt-driven separation process and for removal of heavy metals from salty effluents.

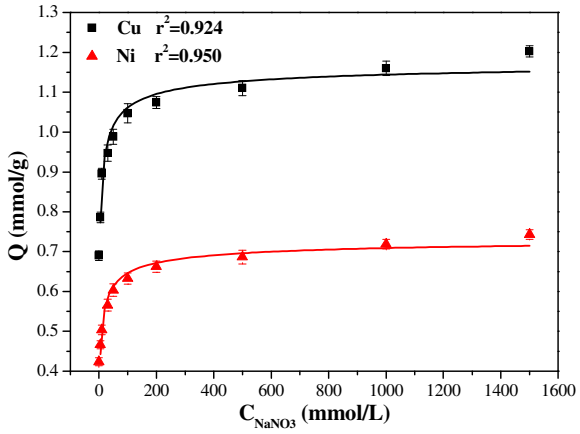

Fig. 9 Adsorption capacity of Cu(II) and Ni(II) in Cu(II)/Na(I) and Ni(II)/Na(I) binary systems with different concentrations of $NaNO_3$.

3.9 Application in treatment of actual waste stream

Given the unique salt-enhanced removal and salt-tuned separation properties, PAMD is potentially eligible for efficiently sequestering and selectively reusing heavy metals from highly salty system. High-saline wastewater (P507 extraction raffinate, pH = 8.3) was taken from New ERA Group Zhejiang New Energy Material Co., Ltd., with the solution parameters summarized in Table 3. Trace amounts of heavy metals such as Ni(II), Co(II), Pb(II) and Cu(II) were contained in the solution, while extremely high concentrations of Ca(II), Mg(II) and Na(I) were also involved. Thus, it was impossible to reduce the concentrations of heavy metal ions to meet the effluent standard only by applying the traditional precipitation method.

Table 3 Metal contents of P507 extraction raffinate (pH = 8.3).

Ions	Ni(II)	Co(II)	Pb(II)	Cu(II)
Initial Concentration (mg/L)	31.5	1.82	0.396	0.31
Discharge standard (mg/L)	0.05	1.0	0.1	0.5
Ions	Fe(II)	Ca(II)	Mg(II)	Na(I)
Initial Concentration (mg/L)	2.61	30.45	3037.5	9589.6
Discharge standard (mg/L)	–	–	–	–

When P507 extraction raffinate passed through the resin column (0.500 g, 2 mL) of PAMD at the speed of 3 BV/h at 303 K, Ni(II), Co(II), Pb(II) and Cu(II) were not detected in the effluent until 330 BV at which Ni(II) was leaked out firstly. In consideration of the discharge standard (Table 3), 330 BV of clean effluent was obtained (Fig. 10). Furthermore, PAMD resins were regenerated by 15% HCl solution (2 BV/h, running for 5 h), and a solution containing high-concentration nickel (6000 mg/L) was recycled. At last, the resin column was washed with the obtained clean water (5 BV/h, operating for 8 h). PAMD remained highly chemically stable after several regenerations. In order to evaluate the decontamination results, commercial polyamine resin S984 was also applied to treat P507 extraction raffinate. As shown in Fig. 10, only 220 BV of effluent met the discharge standard, and Ni(II) was firstly observed. Therefore, PAMD decontaminated and reutilized heavy metals from the actual salty effluent better than S984 did, being consistent with the static and dynamic adsorption results of simlated salty solutions.

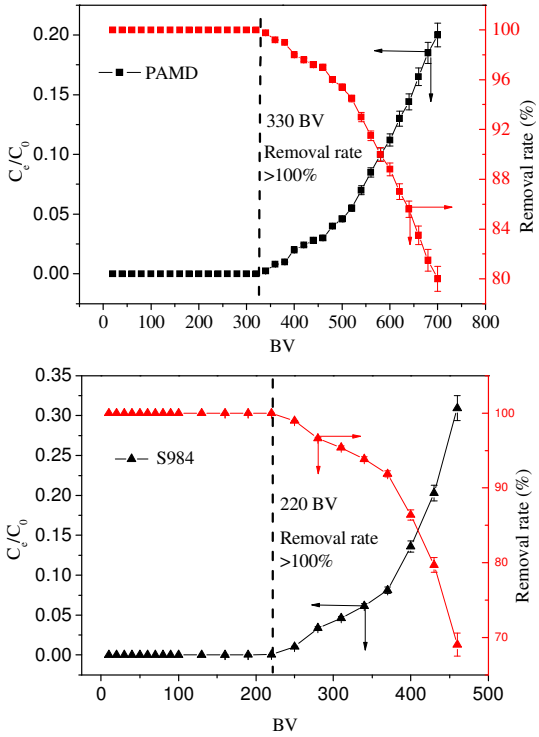

Fig. 10 Breakthrough curves for adsorption of Ni(II) onto PAMD and S984 in the treatment of P507 extraction raffinate.

4. Conclusions

In this study, a novel tetraethylenepentamine functionalized polymeric adsorbent (PAMD) capable of enhanced removal and selective recovery of Cu(II) and Ni(II) from saline solutions was facilely prepared. Due to super-high content of N (20.38%), exceptional binding abilities of amine functional group and multiple chelating sites, the multi-amine adsorbent PAMD exhibited high adsorption capacity and remarkable selectivity towards Cu(II). In Cu(II)/Ni(II)/$NaNO_3$ ternary system, benefiting from positive effect of inorganic salts, the uptake amount of Cu(II) onto PAMD was significantly increased by 73.65%, accompanied by dramatically elevated sorption rate and infinite separation factor. Compared to commercial multi-amine resin S984, PAMD presented a superior efficiency for treatment of actual salty effluents. In brief, we herein provided a low-cost, efficient and environmentally friendly adsorbent (PAMD) for promptly removing and selectively recovering heavy metals in wastewater, especially those in highly saline solution, which have significant potentials in advanced treatment of saline effluents and preparation of high-purity metals.

Acknowledgements

The authors gratefully acknowledge generous support provided by the National Natural Science Foundation of P.R. China (No.51378253) and the Discipline Crossing Foundation of Nanjing University.

Notes and references

1 M. M. Khin, A. S. Nair, V. J. Babu, R. Murugan and S. Ramakrishna, *Energy Environ. Sci.*, 2012, **5**, 8075-8109.

2 D. H. P. Kang, M. Chen and O. A. Ogunseitan, *Environ. Sci. Technol.*, 2013, **47**, 5495-5503.
3 W. Zhang, X. Shi, Y. Zhang, W. Gu, B. Li and Y. Xian, *J. Mater. Chem. A*, 2013, **1**,1745-1753.
4 P. Liu, P. F. Borrell, M. Bozic, V. Kokol, K. Oksman and A. P. Mathew, *J. Hazard. Mater.*, 2015, **294**, 177-185.
5 S.-O. Tung, S. Ho, M. Yang, R. Zhang and N. A. Kotov, *Nat. Commun.*, 2015, **6**, 6152–6158.
6 S. Tominaka, H. Hamoudi, T. Suga, T. D. Bennett, A. B. Cairns and A. K. Cheetham, *Chem. Sci.*, 2015, **6**, 1465-1473.
7 M. Ye, X. Wen, N. Zhang, W. Guo, X. Liu and C. Lin, *J. Mater. Chem. A*, 2015, **3**, 9595-9600.
8 E. J. Popczun, J. R. McKone, C. G. Read, A. J. Biacchi, A. M. Wiltrout, N. S. Lewis and R. E. Schaak, *J. Am. Chem. Soc.*, 2013, **135**, 9267-9270.
9 C. Chen, Y. Kang, Z. Huo, Z. Zhu, W. Huang, H. L. Xin, J. D. Snyder, D. Li, J. A. Herron, M. Mavrikakis, M. Chi, K. L. More, Y. Li, N. M. Markovic, G. A. Somorjai, P. Yang and V. R. Stamenkovic, *Science*, 2014, **343**, 1339-1343.
10 H. Hu, J. H. Xin, H. Hu, X. Wang, D. Miao and Y. Liu, *J. Mater. Chem. A*, 2015, **3**, 11157-11182.
11 F. Tisato, C. Marzano, M. Porchia, M. Pellei and C. Santini, *Med. Res. Rev.*, 2010, **30**, 708-749.
12 Y. C. Shih, C. Y. Ke, C. J. Yu, C. Y. Lu and W. L. Tseng, *ACS Appl. Mater. Interfaces*, 2014, **6**, 17437-17445.
13 Y. Su, A. S. Adeleye, Y. Huang, X. Sun, C. Dai, X. Zhou, Y. Zhang and A. A. Keller, *Water Res.*, 2014, **63**, 102-111.
14 G. Zeng, Y. Liu, L. Tang, G. Yang, Y. Pang, Y. Zhang, Y. Zhou, Z. Li, M. Li, M. Lai, X. He and Y. He, *Chem. Eng. J.*, 2015, **259**, 153-160.
15 O. Shvets and L. Belyakova, *J. Hazard. Mater.*, 2015, **283**,643-656.
16 W. Li, S. Gao, L. Wu, S. Qiu, Y. Guo, X. Geng, M. Chen, S. Liao, C. Zhu, Y. Gong, M. Long, J. Xu, X. Wei, M. Sun and L. Liu, *Sci. Rep.*, 2013, **3**, 2125-2130.
17 L. Wang, C. Cheng, S. Tapas, J. Lei, M. Matsuoka, J. Zhang and F. Zhang, *J. Mater. Chem. A*, 2015, **3**, 13357-13364.
18 A. E. Kandjani, Y. M. Sabri, M. Mohammad-Taheri, V. Bansal and S. K. Bhargava, *Environ. Sci. Technol.*, 2015, **49**, 1578-1584.
19 X. Tan, Y. Liu, G. Zeng, X. Wang, X. Hu, Y. Gu and Z. Yang, *Chemosphere*, 2015, **125**, 70-85.
20 V. K. Sharma, R. Zboril and R. S. Varma, *Acc. Chem. Res.*, 2015, **48**, 182-191.
21 C. Ling, F. Q. Liu, C. Xu, T. P. Chen and A. M. Li, *ACS Appl. Mater. Interfaces*, 2013, **5**, 11808-11817.
22 J. Han, Z. Cao and W. Gao, *J. Mater. Chem. A*, 2013, *1*, 4941-4944.
23 S. Ma, Q. Chen, H. Li, P. Wang, S. M. Islam, Q. Gu, X. Yang and M. G. Kanatzidis, *J. Mater. Chem. A*, 2014, **2**, 10280-10289.
24 M. Ceglowski and G. Schroeder, *Chem. Eng. J.*, 2015, **263**, 402-411.
25 Y. Shen and B. Chen, *Environ. Sci. Technol.*, 2015, **49**, 7364-7372.
26 Y. Huang and A. A. Keller, *Water Res.*, 2015, **80**, 159-168.
27 Q. Zhang, J. Teng, Z. Zhang, G. Nie, H. Zhao, Q. Peng and T. Jiao, *Rsc Adv.*, 2015, **5**, 55445-55452.
28 M. X. Tan, Y. N. Sum, J. Y. Ying and Y. Zhang, *Energy Environ. Sci.*, 2013, **6**, 3254-3259.
29 H. T. Xing, J. H. Chen, X. Sun, Y. H. Huang, Z. B. Su, S. R. Hu, W. Weng, S. X. Li, H. X. Guo, W. B. Wu, Y. S. He, F. M. Li and Y. Huang, *Chem. Eng. J.*, 2015, **263**, 280-289.
30 W. Peng, Z. Xie, G. Cheng, L. Shi and Y. Zhang, *J. Hazard. Mater.*, 2015, **294**, 9-16.
31 Y. Chen, J. Chen, S. Chen, K. Tian and H. Jiang, *J. Mater. Chem. A*, 2015, **3**, 9843-9850.
32 J. B. Linden, M. Larsson, S. Kaur, W. M. Skinner, S. J. Miklavcic, T. Nann, I. M. Kempson and M. Nyden, *Rsc Adv.*, 2015, **5**, 51883-51890.
33 Y. Chen, M. He, C. Wang and Y. Wei, *J. Mater. Chem. A*, 2014, **2**, 10444-10453.
34 T. Wang, L. Zhang, C. Li, W. Yang, T. Song, C. Tang, Y. Meng, S. Dai, H. Wang, L. Chai and J. Luo, *Environ. Sci. Technol.*, 2015, **49**, 5654-5662.
35 W. Chouyyok, Y. Shin, J. Davidson, W. D. Samuels, N. H. Lafemina, R. D. Rutledge, G. E. Fryxell, T. Sangvanich and W. Yantasee, *Environ. Sci. Technol.*, 2010, **44**, 6390-6395.
36 L. F. Koong, K. F. Lam, J. Barford and G. McKay, *J. Colloid Interface Sci.*, 2013, **395**, 230-240.
37 B. Qiu, J. Guo, X. Zhang, D. Sun, H. Gu, Q. Wang, H. Wang, X. Wang, X. Zhang, B. L. Weeks, Z. Guo and S. Wei, *ACS Appl. Mater. Interfaces*, 2014, **6**, 19816-19824.
38 C. Xu, F.-Q. Liu, J. Gao, L.-J. Li, Z.-P. Bai, C. Ling, C.-Q. Zhu, D. Chen and A.-M. Li, *J. Hazard. Mater.*, 2014, **280**, 1-11.
39 C.-Q. Zhu, F.-Q. Liu, C. Xu, J. Gao, D. Chen and A.-M. Li, *J. Hazard. Mater.*, 2015, **287**, 234-242.
40 R. R. Navarro, K. Tatsumi, K. Sumi and M. Matsumura, *Water Res.*, 2001, **35**, 2724-2730.
41 J. Ma, F. Yu, L. Zhou, L. Jin, M. Yang, J. Luan, Y. Tang, H. Fan, Z. Yuan and J. Chen, *ACS Appl. Mater. Interfaces*, 2012, **4**, 5749-5760.
42 J. Huang, L. Yang, Y. Zhang, C. Pan and Y.-N. Liu, *Chem. Eng. J.*, 2013, **219**, 238-244.
43 P. X. Sheng, Y. P. Ting and J. P. Chen, *Ind. Eng. Chem. Res.*, 2007, **46**, 2438-2444.
44 S. K. Papageorgiou, F. K. Katsaros, E. P. Kouvelos and N. K. Kanellopoulos, *J. Hazard. Mater.*, 2009, **162**, 1347-1354.
45 C. Mahamadi and T. Nharingo, *Bioresoure Technol.*, 2010, **101**, 859-864.
46 X. Li, L. Yang, Y. Li, Z. Ye and A. He, *J. Environ. Eng.*, 2012, **138**, 940-948.
47 C. M. F. da Silva, Q. d. C. Rocha, P. C. S. Rocha, A. M. T. Louvisse and E. F. Lucas, *J. Environ. Manage.*, 2015, **157**, 205-212.
48 A. Asfaram, M. Ghaedi, S. Agarwal, I. Tyagi and V. K. Gupta, *Rsc Adv.*, 2015, **5**, 18438-18450.
49 H. A. Abdulla, E. C. Minor and P. G. Hatcher, *Environ. Sci. Technol.*, 2010, **44**, 8044-8049.
50 C. Shen, Y. Shen, Y. Wen, H. Wang and W. Liu, *Water Res.*, 2011, **45**, 5200-5210.
51 X. Guo, S. Zhang and X.-Q. Shan, *J. Hazard. Mater.*, 2008, **151**, 134-142.
52 J. He, H.-X. Xue, C.-W. Lue, Q.-Y. Fan, Y. Liang, Y. Sun, L.-L. Shen and S. Bai, *Environ. Geol.*, 2009, **58**, 1499-1508.
53 L. Bai, H. Hu, W. Zhang, J. Fu, Z. Lu, M. Liu, H. Jiang, L. Zhang, Q. Chen and P. Tan, *J. Mater. Chem.*, 2012, **22**,17293-17301.
54 L. Li, F. Liu, X. Jing, P. Ling and A. Li, *Water Res.*, 2011, **45**, 1177-1188.
55 C. Liu, R. Bai and Q. S. Ly, *Water Res.*, 2008, **42**, 1511-1522.
56 J. Gao, F. Liu, P. Ling, J. Lei, L. Li, C. Li and A. Li, *Chem. Eng. J.*, 2013, **222**, 240-247.
57 K. F. Lam, X. Chen, G. McKay and K. L. Yeung, *Ind. Eng. Chem. Res.*, 2008, **47**, 9376-9383.
58 C. Liu, R. Bai and L. Hong, *J. Colloid Interface Sci.*, 2006, **303**, 99-108.
59 K. Bourikas, C. Kordulis, J. Vakros and A. Lycourghiotis, *Adv. Colloid Interface Sci.*, 2004, **110**, 97-120.
60 P. F. Luckham and S. Rossi, *Adv. Colloid Interface Sci.*, 1999, **82**, 43-92.
61 O. Stern, *Z. Elektrochem. Angew. Phys. Chem.*, 1924, **30**, 508-516.
62 C. Y. Tang, Q. S. Fu, D. Gao, C. S. Criddle and J. O. Leckie, *Water Res.*, 2010, **44**, 2654-2662.
63 F. Xiao, X. Zhang, L. Penn, J. S. Gulliver and M. F. Simcik, *Environ. Sci. Technol.*, 2011, **45**, 10028-10035.